Research Article
doi.org/10.1002/cctc.202300350

www.chemcatchem.org

An Amorphous Teflate Doped Aluminium Chlorofluoride: A Solid Lewis-Superacid for the Dehydrofluorination of Fluoroalkanes

Minh Bui,[a] Kurt F. Hoffmann,[b] Thomas Braun,*[a] Sebastian Riedel,*[b] Christian Heinekamp,[a, c] Kerstin Scheurell,[a] Gudrun Scholz,[a] Tomasz M. Stawski,[c] and Franziska Emmerling[a, c]

An anion-doped aluminium chlorofluoride $AlCl_{0.1}F_{2.8}(OTeF_5)_{0.1}$ (ACF-teflate) was synthesized. The material contains pentafluoroorthotellurate (teflate) groups, which mimic fluoride ions electronically, but are sterically more demanding. They are embedded into the amorphous structure. The latter was studied by PDF analysis, EXAFS data and MAS NMR spectroscopy. The mesoporous powder is a Lewis superacid, and ATR-IR spectra of adsorbed CD_3CN reveal a blue-shift of the adsorption band by 73 cm^{-1}, which is larger than the shift for SbF_5. Remarkably, ACF-teflate catalyzes dehydrofluorination reactions of monofluoroalkanes to yield olefins in C_6D_6. In these cases, no Friedel-Crafts products were formed.

Introduction

Amorphous aluminium fluoride-based catalysts can be considered as very strong Lewis-acids.[1] Nanoscopic aluminium chlorofluoride (ACF, $AlCl_xF_{3-x}$, with $x = 0.3-0.05$) exhibits a Lewis-acidity comparable to SbF_5.[1c,2] It has been synthesized by fluorination of $AlCl_3$ with CCl_3F and applied in a variety of conversions such as C–H activation, fluorination, defluorination or Friedel-Crafts type conversions.[3] Especially hydrodefluorination type reactions can be promoted by the presence of silanes and silylium-type surface species might play a crucial role to induce the C–F bond cleavage reactions.[3c,4] A variety of other Lewis-acidic amorphous aluminium fluoride catalyst were developed such as the mesoscopic *high-surface*-AlF_3.[5] Fluorination of γ-Al_2O_3-700 with $CHClF_2$ also gives a highly Lewis-acidic mesoporous catalyst.[6] In the presence of Et_3SiH dehydrofluorination of fluoropentane was found, albeit with very low selectivity. A Nb doped Al hydroxide fluoride was obtained by reaction of Al isopropoxide with aqueous HF, and post-fluorination of the produced xerogel with $CHClF_2$ at higher temperatures. It is also mesoscopic, but shows Lewis-acidic and Brønsted-acidic properties.[7] In all of these materials Lewis-acidity and amorphicity are mainly due to the distortion of the bulk structure by chloride or isopropoxide groups. Note also that recently a heterogeneous Al-based Lewis Acid was generated by treatment of partially dehydroxylated silica with $Al(OC(CF_3)_3)_3(PhF)$.[8]

The pentafluoroorthotellurate group ($[OTeF_5]^-$, teflate group) is an interesting substitute for fluoride, because the teflate group mirrors the electron withdrawing properties of fluoride, but it is considerably bulkier.[9] It can be considered as chemical inert towards electrophiles. The monomeric aluminium teflate $Al(OTeF_5)_3$ exhibits a much higher Lewis acidity compared to the one of SbF_5.[10] However, a dimeric structure $[Al(OTeF_5)_3]_2$ in the solid state has been suggested, which lowers the Lewis acidity.[11] Nevertheless, it can be regarded as a soluble molecular counterpart of AlF_3 phases.[12]

Herein, we report on an unprecedented strategy to design properties of an aluminium fluoride. Controlled anion-doping with teflate groups by using $[Al(OTeF_5)_3]_2$ yielded an amorphous aluminium chlorofluoride (ACF-teflate). The sterically demanding $[OTeF_5]^-$ moieties preset a pronounced distortion of the bulk material, which induces Lewis superacidity. As a result, ACF-teflate is an active catalyst for the dehydrofluorination of fluoroalkanes at room temperature to yield olefins.

Results and Discussion

Fluorination of a mixture of $AlCl_3$ and 5 mol% $Al(OTeF_5)_3$ by treatment with $CFCl_3$ at low temperature was achieved to obtain a pale yellow powder after removal of the generated CCl_4 [Equation (1)]. The surface properties of ACF-teflate were

[a] M. Bui, Prof. Dr. T. Braun, C. Heinekamp, Dr. K. Scheurell, Dr. G. Scholz, Priv.-Doz. Dr. F. Emmerling
Department of Chemistry
Humboldt-Universität zu Berlin
Brook-Taylor-Straße 2, D-12489 Berlin (Germany)
E-mail: thomas.braun@chemie.hu-berlin.de
[b] K. F. Hoffmann, Prof. Dr. S. Riedel
Institut für Chemie und Biochemie
Freie Universität Berlin
Fabeckstraße 34/36
D-14195 Berlin (Germany)
E-mail: s.riedel@fu-berlin.de
[c] C. Heinekamp, Dr. T. M. Stawski, Priv.-Doz. Dr. F. Emmerling
BAM Federal Institute for Materials Research and Testing
Richard-Willstätter-Straße 11
D-12489 Berlin (Germany)

Supporting information for this article is available on the WWW under https://doi.org/10.1002/cctc.202300350

assessed by gas N_2 adsorption experiments and BET analysis. The adsorption isotherm for ACF-teflate features at low pressure a type II like shape. A type H4 hysteresis indicates slit-like pores on the surface (see SI).[13] ACF-teflate is mesoporous and BJH analysis reveals a larger pore size (31 Å) than in ACF (12 Å), but a smaller surface area (220 $m^2 g^{-1}$ vs 330 $m^2 g^{-1}$ for ACF).[14]

$$AlCl_3 + 0.05\ Al(OTeF_5)_3 \xrightarrow[2h,\ -30°C\ -\ CCl_4]{\text{excess of } CCl_3F} \underset{\text{ACF-teflate}}{AlCl_{0.1}F_{2.8}(OTeF_5)_{0.1}} \quad (1)$$

Powder XRD studies revealed an amorphous nature for ACF-teflate. In the DSC profile an exothermic event was observed at approximately 450 °C, which indicates a crystallization process (see SI). TGA shows a mass loss in a range from 100 until 300 °C, whereas at 180 °C sublimation of $AlCl_3$ sets in. After heating up to 600 °C a mass loss of nearly 16% was detected. Powder XRD data that were measured after heating, were assigned to β-AlF_3, as it was also found for ACF.[15]

STEM measurements at ACF-teflate reveal agglomerates consisting of spherical particles. The sizes of the agglomerates are in a range of 1–2 μm, whereas the single particles have a diameter of approximately 50 nm. Energy dispersive X-ray (EDX) analysis and elemental mappings (Figure 1) disclose that Al, Cl, F, O and Te are distributed homogenously over the entire agglomerate. This confirms the implementation of tellurium containing entities into the ACF structure. The EDX analysis suggests a chemical formula for the ACF-teflate of $AlCl_{0.1}F_{2.8}(OTeF_5)_{0.1}$.

MAS NMR data for ACF-teflate were measured and compared with those of ACF and $[Al(OTeF_5)_3]_2$. The latter were not reported before. The ^{27}Al MAS NMR spectrum for ACF-teflate shows a broad signal at −16 ppm, which is typical for strongly distorted [AlF_6] moieties.[16] This signal has an increased line width by 150 Hz compared to the signal for ACF, suggesting a higher disorder and amorphicity.[17] A minor signal at 44 ppm was observed at a characteristic shift for [AlX_4] entities, where X are either oxygen or fluorine atoms.[18] In the ^{27}Al MAS NMR spectrum of $[Al(OTeF_5)_3]_2$ a signal in the range between 34 and −18 ppm was observed, with a shape typically associated with a second order quadrupolar coupling (see SI). DMFIT was used to determine an isotropic chemical shift ($\delta_{iso}(^{27}Al)$) of about 59 ppm, which is a characteristic value for fourfold coordinated aluminium species. This also confirms the dimeric structure $[Al(OTeF_5)_3]_2$ in the solid state. A ^{19}F MAS NMR spectrum of ACF-teflate shows three signals at −164, −47 and −42 ppm (Figure 2). The very broad signal at −164 ppm can be assigned to distorted [AlF_6] octahedra. The resonance shows an increase of the line width by approximately 700 Hz when compared to the signal for ACF (δ: −167 ppm),[2b,16a] indicating a higher degree of disorder for ACF-teflate. The fairly sharp signal at −47 ppm with a shoulder at −42 ppm suggests the presence of two types of teflate groups. $[Al(OTeF_5)_3]_2$ also shows two distinct signals in the ^{19}F NMR spectrum at −34 and −46 ppm with an intensity ratio of nearly 1:2, presumably for bridging and terminal teflate groups (Figure 2). Finally, spin-echo ^{19}F MAS NMR experiments of ACF-teflate were measured to investigate the chemical environment of the teflate groups in the bulk. By increasing the dipolar evolution time, the signals for the teflate groups remain sharp, which suggests a lower dipolar interaction with their environment. The spin-echo experiments did also reveal a small signal at −195 ppm, which is indicative for the presence of surface bound terminal fluorides (see SI).[2b,16a]

The amorphous nature of ACF-teflate and, for comparison, also ACF were then further investigated by synchrotron-based total scattering measurements at a wavelength of 0.161669 Å (76.7 keV). The pair distribution functions (PDF) displayed in Figure 3 confirm the amorphous and highly-disordered nature of both materials, since any structural coherence is below $r = 4$ Å. This is in contrast to crystalline $AlCl_3$ and AlF_3 samples, for which the coherence extends far beyond 4 Å (Figure 3, black lines). In addition, no distinct Al–Cl bond separations can be estimated from the PDF for ACF and ACF-teflate.

ACF-teflate reveals a peak for Al···F separations at octahedral coordinated Al centers at 1.82 Å. The peak can also partially be contributed by the Te···F bonds of the teflate groups, for which distances are reported between 1.82–1.84 Å.[11] In contrast, ACF displays a broader feature, which seems to be due to two

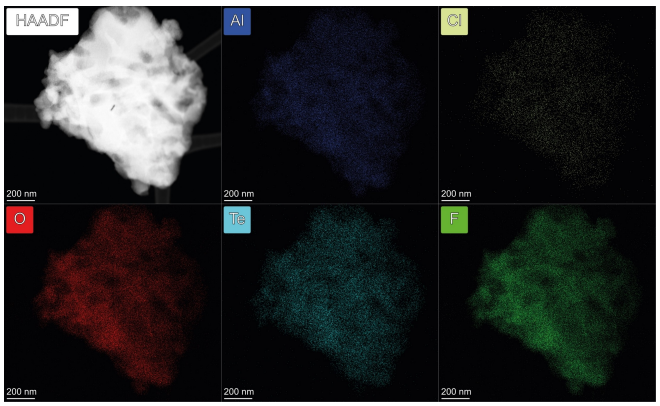

Figure 1. Elemental Mapping of ACF-teflate by STEM and EDX analysis.

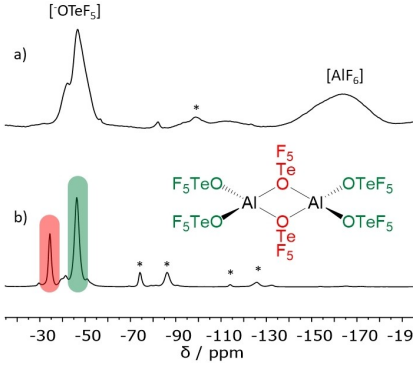

Figure 2. ^{19}F MAS NMR spectra for a) ACF-teflate ($\bar{\nu}_{rot}$: 20 kHz) and for b) $[Al(OTeF_5)_3]_2$ ($\bar{\nu}_{rot}$: 15 kHz). Asterisks (*) represent spinning sidebands; Lewis structure of $[Al(OTeF_5)_3]_2$ with bridging (red) and terminal (green) $[OTeF_5]^-$ groups.

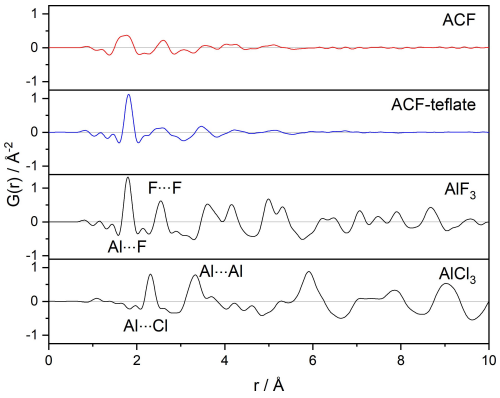

Figure 3. Pair Distribution Functions (PDF) of ACF, ACF-teflate, commercial AlF_3 and $AlCl_3$ from High-Energy X-ray Diffraction (HEXD, wavelength 0.161669 Å) data obtained at I15-1 Diamond Light Source.

overlapping atomic distances at 1.6 and 1.8 Å. No shoulder can be detected for the peak shape at 1.82 Å for ACF-teflate. This indicates that the reported coordination distances in $[OTeF_5]^-$ groups are still intact, which is intriguing.

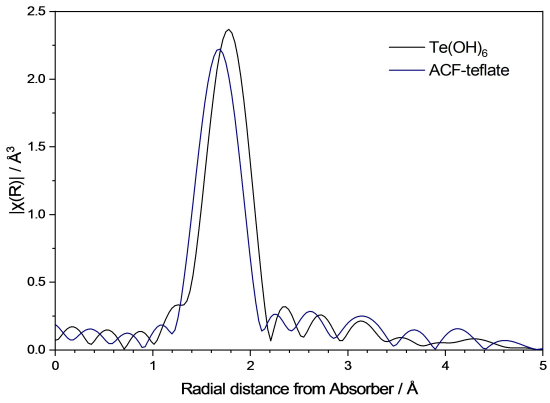

Figure 4. Magnitude of χ in real space from normalized Te K-edge data at 31831.7 eV of ACF-teflate and $Te(OH)_6$.

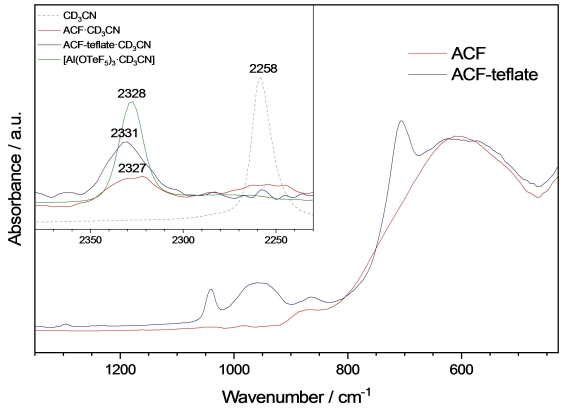

Figure 5. ATR-IR spectra of neat ACF and ACF-teflate. Inset of ATR-IR spectra for CD_3CN as well as CD_3CN loaded ACF, ACF-teflate and $[Al(OTeF_5)_3(CD_3CN)]$.

Extended X-ray absorption fine structure (EXAFS) data at the Te K-edge at 31831.7 eV investigating the teflate coordination sphere are consistent with the PDF data. The magnitude plot of χ in real space depicts a shift of 0.08 Å for ACF-teflate compared to the $Te(OH)_6$ reference sample (Figure 4). The bond separation for ACF-teflate was calculated to be 1.82 Å, which is in accordance with the reported Te···F distances in crystal structures of $[OTeF_5]^-$ containing compounds.[11] The distance Te···O in $Te(OH)_6$ was determined to be 1.92 Å, which fits well with the literature value of 1.91 Å.[19] One cannot differentiate between Te···O and Te···F distances, due to the comparable electron densities of oxygen and fluorine atoms. However, both data sets are in accordance with an octahedral coordination sphere at tellurium.

To confirm the presence of teflate-like groups, ATR-IR spectra were measured (Figure 5). A very broad band at 608 cm^{-1} can be assigned to Al–F entities, as it was also found for ACF. Additionally, a band for Te–F moieties was found at 705 cm^{-1} as well as Al–O vibrational bands at 986 and 1040 cm^{-1}.[11] The band at 863 cm^{-1} can also be due to an Al–O entity.

Infrared spectroscopic data of adsorbed CD_3CN can be used to assess Lewis-acidic sites at the surfaces. For comparison ATR-IR spectra of molecular CD_3CN and $[Al(OTeF_5)_3(CD_3CN)]$ as well as CD_3CN loaded ACF, and ACF-teflate are depicted in Figure 5. The C≡N vibrational band of CD_3CN was observed at 2258 cm^{-1} and serves as reference point for the materials. The band of ACF-teflate loaded with CD_3CN appears at 2331 cm^{-1}, which corresponds to a blue-shift of 73 cm^{-1}. Thus ACF-teflate can be classified as Lewis superacid, as it possesses a higher Lewis acidity than molecular SbF_5.[20]

NH_3-TPD experiments were used to derive information on the nature of acidic surface sites. The TPD profile of ACF-teflate (see SI) shows peaks between 180 °C and 210 °C, between 230 °C and 270 °C and in the range between 270 °C and 350 °C, which can be attributed to weak, medium/strong and strong Lewis-acidic sites, respectively.[14] The peak intensity ratio is 1:2:8, indicating a predominately presence of strong acidic sites at the surface.

To evaluate the catalytic activity of the ACF-teflate, the isomerization of 1,2-dibromohexafluoropropane into 2,2-dibromohexafluoropropane was tested. The reaction is typically catalyzed by strongly Lewis-acidic centers,[5,21] and for ACF-teflate a conversion of 70% at room temperature within 2 h was obtained.

ACF-teflate was then used as catalyst for C–F bond activation reactions. A dehydrofluorination of 1-fluoropentane or 1-fluoroheptane was observed in the presence of Et_3SiH or Et_3GeH to yield H_2 as well as 2-*E/Z*-pentene and the *E/Z* isomers of 2- and 3-heptene, respectively (Scheme 1). It is exceptional that the conversions occur at room temperature, although dehydrofluorination steps at ACF/Et_3GeH were reported at higher temperature.[3b] Interestingly, when the reactions were performed in C_6D_6 an initial dehydrofluorination was seen, but after 24 h the formation of Friedel-Crafts products can also be observed. Remarkably, on using Et_3GeH as hydrogen source

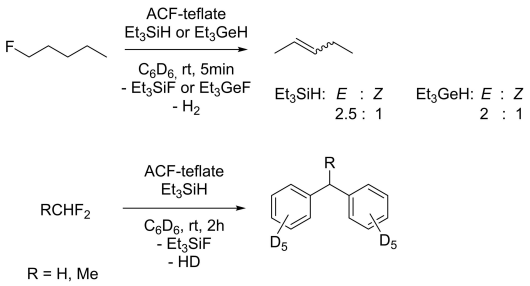

Scheme 1. Catalytic reactions at ACF-teflate; a catalytic reaction of 1-fluoroheptane gives *E/Z* isomers of 2- and 3-heptene.

resulted in dehydrofluorination, regardless if the reaction proceeded in neat germane or in C_6D_6.

Mechanistically, it is feasible to assume that carbenium-like species might play a role as intermediates.[22] They can be generated initially or by reaction with silylium/germylium-type ions.[3a–c,23] The latter are formed after an interaction of silanes or germanes at the ACF-teflate surface. A reaction with fluoroalkanes would then result in C–F bond cleavage to give the fluorosilane or fluorogermane and carbenium-type ions, which can undergo Wagner-Meerwein rearrangements. Subsequently, in the presence of the hydrogen source dihydrogen and the olefinic products are formed. Though, with difluoromethane and 1,1-difluoroethane, the Friedel-Crafts products were observed (Scheme 1), which supports the assumption for the presence of intermediate carbenium-like species. Note that molecular Al(I) complexes can undergo a C–F bond cleavage of fluoroalkenes by oxidative addition to form organoaluminium fluorides.[24] Ichikawa and co-workers reported on a cyclisation of 1-fluoronaphthalenes *via* aromatic C–F bond activation induced by Al(III) reagents.[25]

To gain more insight on the observed reactivities, ACF-teflate samples were loaded with Et_3SiH or fluoropentane. A mass gain of 8% or 3%, respectively, was determined after removal of excess silane under vacuum. This indicates a preference for silane binding over fluoroalkane immobilization. In order to estimate the interaction of silane with ACF-teflate, the latter was treated with silane and the properties of the resulting silane-loaded material was studied spectroscopically. In the ^{27}Al MAS NMR spectrum a signal at −16 ppm was observed that shows an increased line width by 150 Hz when compared to the signal for ACF-teflate, which indicates a slightly less ordered aluminium fluoride matrix. In the ^{19}F MAS NMR spectrum the signal for the teflate groups at −47 ppm and its shoulder at −42 ppm can still be detected, which suggests that immobilization of Et_3SiH at ACF-teflate has no significant influence on its bulk structure. Spin-echo experiments did not show the presence of terminal fluorine atoms anymore. The ^{1}H-^{19}Si CP MAS NMR spectrum exhibits three signals at 74, 38 and 10 ppm, presumably corresponding to a silylium-like species, Et_3SiF and Et_2SiF_2, respectively (see SI).[26]

Conclusion

In conclusion, a unique mesoscopic, amorphous Lewis superacid was synthesized by doping an aluminium chlorofluoride with sterically demanding teflate anions. Such an anion doping with large groups is exceptional for the synthesis of aluminium fluoride materials. The $[OTeF_5]^-$ moieties seem to remain their identity in the bulk structure, which leads presumably to highly distorted structure. As a consequence, ACF-teflate is highly Lewis acidic and catalyzes dehydrofluorination reactions of fluoroalkanes at room temperature, which is very unique. The reported synthetic approach to a new class of doped ACF derivatives could pave the way for further modifications and improvements of ACF-based acidic catalysts.

Experimental Section

General techniques, procedures and materials

The samples were prepared in a MBraun glovebox and all reactions were performed in J Young NMR tubes using conventional Schlenk techniques. C_6D_6 was purchased from Eurisotop, dried over K-Solvona and distilled before usage. CD_3CN was obtained from Sigma-Aldrich and used as received. Triethylsilane, triethylgermane, 1-fluoropentane and 1-fluoroheptane were purchased from Sigma-Aldrich and stored under an argon atmosphere and molecular sieve in Schlenk flasks. Aluminiumchloride was purified by sublimation before usage. The gases difluoromethane and 1,1-difluoroethane were purchased from ABCR.

Liquid NMR spectra were measured at a Bruker DPX 300, Bruker AVANCE II 300 or a Bruker AVANCE II 500 spectrometer at room temperature with tetramethylsilane as external standard. ^{1}H NMR chemical shifts δ were referenced to residual C_6D_5H (δ = 7.16 ppm). ^{19}F NMR spectra were calibrated externally to $CFCl_3$ (δ = 0 ppm) and ^{13}C NMR spectra were referenced to C_6D_6 (δ = 128.06 ppm). All conversions were determined by ^{1}H NMR spectroscopy with $PhCF_3$ as internal standard. The yields for the dehydrofluorination reactions were calculated based on the conversion of fluoroalkanes into the olefines. The ratio of the isomers for the dehydrofluorination reactions were calculated by ^{1}H NMR spectroscopy. For the Friedel Crafts type reactions the yields were determined based on the conversion of fluoroalkanes into the Friedel-Crafts products.

Solid-state MAS (magic angle spinning) nuclear magnetic resonance spectra were recorded at a Bruker AVANCE 400 (B_0 = 9.4 T) spectrometer at room temperature. Depending on the nucleus different rotor sizes were used: 2.5 mm rotors for ^{1}H, ^{19}F and ^{27}Al; 4 mm for ^{1}H-^{29}Si CP and ^{125}Te. The chemical shifts are given with respect to a $CFCl_3$ standard for ^{19}F and an aqueous solution of $AlCl_3$ for ^{27}Al. For both nuclei AlF_3 was used as external standard. ^{125}Te NMR spectra were referenced to $Te(CH_3)_2$ and $Te(OH)_6$ as an external standard. The respective Larmor frequencies are ν_{1H} = 400.1 MHz, ν_{13C} = 100.6 MHz, ν_{19F} = 376.4 MHz, ν_{27Al} = 104.3 MHz, ν_{29Si} = 79.5 MHz and ν_{125Te} = 126.2 MHz. The ^{1}H 90° pulse length was set as 2.6 μs. The contact time was 3 or 8 ms and the d1 time was 5 s. The ^{1}H-^{29}Si CP MAS NMR spectra were recorded by using a ^{1}H 90° pulse length of 2.65 μs at 6 dB while the contact time was 5 ms and d1 time was 5 s. As external standard Na_2SiF_6 (^{29}Si = 189.1 ppm) was used.

X-ray powder diffraction measurements were performed on an STOE Stadi MP diffractometer equipped with a Dectris Mythen 1 K

linear silicon strip detector and Ge(111)double-crystal monochromator (Mo–K radiation) in a transmission geometry.

The IR-spectra were recorded in a glovebox at a Bruker Alpha II spectrometer with a diamond ATR (attenuated total reflectance) measuring unit (Pyroelectric DTGS detector).

Low temperature adsorption isotherms of nitrogen at 77 K were determined with a Micro-meritics ASAP 2020. Approximately 150 mg of the samples were tempered at 150 °C for 10 h immediately before the measurement at the device.

High-energy X-ray diffraction (HEXD) measurements were performed at the beamline I15-1 of the Diamond Light Source (UK). The diffraction patterns were collected at 76 keV, which corresponded to a wavelength of 0.161669 Å. The 2D patterns were measured with a Perkin Elmer XRD 1611 CP3 detector (409.6·409.6 mm^2 active area, 100 μm pixel size) in Debye-Scherrer geometry. The powder samples were measured in spinning capillaries using the standard I15-1 setup. The q-range was calibrated using a CeO_2 standard. Dark current contributions were corrected automatically by the acquisition software. The as-obtained 2D patterns were reduced to raw 1D curves using DAWN. The atomic pair distribution functions (PDFs) was obtained from the diffraction patterns using the PDFgetX3 software,[27] which was also used for the background and Compton scattering subtractions. Further analysis was performed in Python using a DiffPy library.

EXAFS measurements were performed at the BAM*line* at BESSY-II.[28] The beam was monochromatized using a double-crystal monochromator (DCM) installed at the beamline, with a resolution (ΔE/E) of about $2 h \cdot 10^{-4}$. The slits were adjusted to provide a 4 mm (H)·1 mm (V) spot size. The measurements were performed @ Te K-edge (31.814 keV) in transmission, as the sample preparation allowed choosing the adequate thickness for optimal absorption, establishing an edge jump factor of about 2. This was achieved by diluting the powder samples with boron nitride. The excitation energy was varied from −200 to −20 eV below the edge in 10 eV steps, from −20 eV below the edge and 200 eV above the edge in 1 eV steps, and in the EXAFS region with a constant step in the *k*-space of 0.04 $Å^{-1}$ until $k = 16$ Å. EXAFS data were processed by ATHENA and ARTEMIS.[29] This GUI programs are part of the main package IFEFFIT (v. 1.2.12). The AutoBK background subtraction procedure was used with the Rbkg parameter set to 1.0 Å and kw = 1. Afterwards all spectra were normalized to the far post-edge region, free from absorption features. Regarding the EXFAS region, with ATHENA one can plot $\chi(k)$ against R(Å) and the oscillations represent different frequencies, which correspond to the different distances for each coordination shell. Hence, Fourier transforms (FT) are necessary for the analysis process. The FT from the k-space to R-space were performed with a Hanning-type window with a range of 1.5 to 14 Å. By analyzing the signal in the frequency domain in ATHENA the window range was selected to exclude the noisy part of the signal.

High-resolution transmission electron microscopy (HRTEM), high-angle annular dark-field scanning transmission electron microscopy (HAADF-STEM) and energy dispersive X-ray analysis (EDX) elemental mapping were carried out on a FEI Talos F200S scanning/transmission electron microscope (S/TEM) at an acceleration voltage of 200 kV. A dry TEM grid preparation was carried out. Therefore, TEM grids were carefully swiped across the powder samples. The excess of powder on the grids were removed by tapping lightly.

The TGA and DSC measurements were performed on a TGA/DSC 3+ from Mettler Toledo, Switzerland. Samples were weight in in a glovebox and sealed with the A2 closing stamp. The closed crucible was pinned in a N_2 stream by the sample robot. The samples were heated from 25 to 600 °C at a rate of 10 K/min. Afterwards the samples were cooled down to 25 °C at the same rate.

NH_3-TPD were performed on the Autosorb iQ equipped with a TCD detector from Anton Paar. Approximately 200 mg of the sample were placed between two layers of quartz wool in a quartz cell. The cell was evacuated for 20 min and then tempered to 150 °C with a heating rate of 5 K/min while in a helium flow. Then, the cell was cooled down to 120 °C and NH_3 gas was added for 15 min. After that, the gas flow was changed again to helium and the detector was turned on. Helium was then flowed for 30 min to get rid of the non-adsorbed NH_3 on the sample surface. The TPD measurement was then performed starting at 80 °C until 500 °C with a heating rate of 5 K/min.

Synthesis of ACF-teflate

$AlCl_3$ (eq, 10.6 mmol, 1400 mg) and $Al_2(OTeF_5)_6$ (0.54 mmol, 400 mg)[10] were placed in a round Schlenk flask and cooled down to −30 °C. Then CCl_3F (53 mmol) was condensed onto the mixture. The resulting yellowish suspension was stirred for 1 h at −30 °C, and then for 2 h at 25 °C. A yellow powder in was obtained after removal of the solvent under vacuum.

Formation of ACF-teflate·CD_3CN and ACF·CD_3CN

ACF-teflate or ACF (200 mg) were suspended in an excess of CD_3CN in a Schlenk flask and stirred at 25 °C for two hours. The excess of CD_3CN was removed under vacuum to obtain a brown powder.

Reactivity studies towards liquid fluoroalkanes (1-fluoropentane, 1-fluoroheptane)

15 mg of ACF-teflate were placed in a J Young NMR tube and Et_3SiH (0.2 mmol) was added resulting in a dark suspension. Then, the fluoroalkane (0.2 mmol) was added and gas evolution was observed. After that C_6D_6 was added to the reaction mixture. The products were analyzed by NMR spectroscopy (see SI).

Reactivity studies towards gaseous fluoroalkanes (difluoromethane, 1,1-difluoroethane)

In a J Young NMR Tube 15 mg of ACF-teflate was suspended in Et_3SiH (0.2 mmol) resulting in a dark suspension. Then C_6D_6 was added and the mixture as cooled down to −196 °C. Afterwards, the gases were condensed into the reaction mixture.

Acknowledgements

We acknowledge financial support from the CRC 1349 "Fluorine Specific Interactions" funded by the German Research Foundation (project number 387284271). We would like to thank Diamond Light Source for beamtime (proposal CY28776), and the staff of beamline I15-1, in particular Dr. Maria Diaz-Lopez for assistance with the HEXD data collection. In addition, we appreciate the measurement time at BAMline at Bessy II (proposal 221-11074) and Dr. Ana Guilherme Buzanich for conducting the XAS measurement. We also acknowledge support by the German Research Foundation under Germany's Excellence Strategy – EXC 2008 – 390540038 – UniSysCat.We thank Dr. Mike Ahrens for helpful

discussions. Open Access funding enabled and organized by Projekt DEAL.

Conflict of Interest

The authors declare no conflict of interest.

Data Availability Statement

The data that support the findings of this study are available in the supplementary material of this article.

Keywords: aluminium fluorides · aluminium teflates · C–F activation · Lewis superacids · silanes

[1] a) J. L. Delattre, P. J. Chupas, C. P. Grey, A. M. Stacy, *J. Am. Chem. Soc.* **2001**, *123*, 5364–5365; b) H. Bozorgzadeh, E. Kemnitz, M. Nickkho-Amiry, T. Skapin, J. M. Winfield, *J. Fluorine Chem.* **2001**, *107*, 45–52; c) T. Krahl, E. Kemnitz, *Catal. Sci. Technol.* **2017**, *7*, 773–796.
[2] a) Carl G. Krespan, V. A. Petrov, B. E. Smart (DuPont de Nemours), U. S. A. 5416246, **1992**; b) T. Krahl, E. Kemnitz, *J. Fluorine Chem.* **2006**, *127*, 663–678.
[3] a) G. Meißner, K. Kretschmar, T. Braun, E. Kemnitz, *Angew. Chem. Int. Ed.* **2017**, *56*, 16338–16341; *Angew. Chem.* **2017**, *129*, 16556–16559; b) G. Meißner, D. Dirican, C. Jäger, T. Braun, E. Kemnitz, *Catal. Sci. Technol.* **2017**, *7*, 3348–3354; c) M. Ahrens, G. Scholz, T. Braun, E. Kemnitz, *Angew. Chem. Int. Ed.* **2013**, *52*, 5328–5332; *Angew. Chem.* **2013**, *125*, 5436–5440; d) M.-C. Kervarec, C. P. Marshall, T. Braun, E. Kemnitz, *J. Fluorine Chem.* **2019**, *221*, 61–65.
[4] M.-C. Kervarec, E. Kemnitz, G. Scholz, S. Rudić, T. Braun, C. Jäger, A. A. L. Michalchuk, F. Emmerling, *Chem. Eur. J.* **2020**, *26*, 7314–7322.
[5] E. Kemnitz, U. Groß, S. Rüdiger, C. S. Shekar, *Angew. Chem. Int. Ed.* **2003**, *42*, 4251–4254; *Angew. Chem.* **2003**, *115*, 4383–4386.
[6] C. P. Marshall, G. Scholz, T. Braun, E. Kemnitz, *Catal. Sci. Technol.* **2020**, *10*, 391–402.
[7] C. P. Marshall, G. Scholz, T. Braun, E. Kemnitz, *Dalton Trans.* **2019**, *48*, 6834–6845.
[8] K. K. Samudrala, W. Huynh, R. W. Dorn, A. J. Rossini, M. P. Conley, *Angew. Chem. Int. Ed.* **2022**, *61*, e202205745.
[9] a) D. Lentz, K. Seppelt, *Angew. Chem. Int. Ed. Engl.* **1978**, *17*, 355–356; b) T. Birchall, R. D. Myers, H. De Waard, G. J. Schrobilgen, *Inorg. Chem.* **1982**, *21*, 1068–1073.
[10] K. F. Hoffmann, A. Wiesner, S. Steinhauer, S. Riedel, *Chem. Eur. J.* **2022**, *28*, e202201958.
[11] A. Wiesner, T. W. Gries, S. Steinhauer, H. Beckers, S. Riedel, *Angew. Chem. Int. Ed.* **2017**, *56*, 8263–8266; *Angew. Chem.* **2017**, *129*, 8375–8378.
[12] P. Tomar, T. Braun, E. Kemnitz, *Eur. J. Inorg. Chem.* **2019**, *2019*, 4735–4739.
[13] K. S. Sing, *Pure Appl. Chem.* **1985**, *57*, 603–619.
[14] B. Calvo, C. P. Marshall, T. Krahl, J. Kröhnert, A. Trunschke, G. Scholz, T. Braun, E. Kemnitz, *Dalton Trans.* **2018**, *47*, 16461–16473.
[15] T. Krahl, *Dissertation*, Humboldt University Berlin, **2005**.
[16] a) T. Krahl, R. Stösser, E. Kemnitz, G. Scholz, M. Feist, G. Silly, J.-Y. Buzaré, *Inorg. Chem.* **2003**, *42*, 6474–6483; b) R. König, G. Scholz, R. Bertram, E. Kemnitz, *J. Fluorine Chem.* **2008**, *129*, 598–606; c) R. König, G. Scholz, A. Pawlik, C. Jäger, B. Van Rossum, H. Oschkinat, E. Kemnitz, *J. Phys. Chem. C* **2008**, *112*, 15708–15720.
[17] K. Chen, *Int. J. Mol. Sci.* **2020**, *21*, 5666.
[18] a) V. Lacassagne, C. Bessada, P. Florian, S. Bouvet, B. Ollivier, J.-P. Coutures, D. Massiot, *J. Phys. Chem. B* **2002**, *106*, 1862–1868; b) C. Bessada, V. Lacassagne, D. Massiot, P. Florian, J.-P. Coutures, E. Robert, B. Gilbert, *Z. Naturforsch. A* **1999**, *54*, 162–166.
[19] O. Lindqvist, *Acta Chem. Scand.* **1970**, *24*, 3178–3188.
[20] a) B. v. Ahsen, B. Bley, S. Proemmel, R. Wartchow, H. Willner, F. Aubke, *Z. Anorg. Allg. Chem.* **1998**, *624*, 1225–1234; b) L. O. Müller, D. Himmel, J. Stauffer, G. Steinfeld, J. Slattery, G. Santiso-Quiñones, V. Brecht, I. Krossing, *Angew. Chem. Int. Ed.* **2008**, *47*, 7659–7663; *Angew. Chem.* **2008**, *120*, 7772–7776; c) L. Greb, *Chem. Eur. J.* **2018**, *24*, 17881–17896.
[21] a) V. A. Petrov, C. G. Krespan, B. E. Smart, *J. Fluorine Chem.* **1998**, *89*, 125–130; b) C. G. Krespan, V. A. Petrov, *Chem. Rev.* **1996**, *96*, 3269–3302.
[22] a) R. Panisch, M. Bolte, T. Müller, *J. Am. Chem. Soc.* **2006**, *128*, 9676–9682; b) V. J. Scott, R. Çelenligil-Çetin, O. V. Ozerov, *J. Am. Chem. Soc.* **2005**, *127*, 2852–2853; c) C. Douvris, C. M. Nagaraja, C.-H. Chen, B. M. Foxman, O. V. Ozerov, *J. Am. Chem. Soc.* **2010**, *132*, 4946–4953; d) C. Douvris, O. V. Ozerov, *Science* **2008**, *321*, 1188.
[23] M. Talavera, G. Meißner, S. G. Rachor, T. Braun, *Chem. Commun.* **2020**, *56*, 4452–4455.
[24] a) C. Bakewell, A. J. P. White, M. R. Crimmin, *Angew. Chem. Int. Ed.* **2018**, *57*, 6638–6642; *Angew. Chem.* **2018**, *130*, 6748–6752; b) T. Chu, I. Korobkov, G. I. Nikonov, *J. Am. Chem. Soc.* **2014**, *136*, 9195–9202; c) O. Kysliak, H. Görls, R. Kretschmer, *Chem. Commun.* **2020**, *56*, 7865–7868.
[25] N. Suzuki, T. Fujita, K. Y. Amsharov, J. Ichikawa, *Chem. Commun.* **2016**, *52*, 12948–12951.
[26] a) H. F. T. Klare, M. Oestreich, *Dalton Trans.* **2010**, *39*, 9176–9184; b) A. Martens, O. Petersen, H. Scherer, I. Riddlestone, I. Krossing, *Organometallics* **2018**, *37*, 706–711; c) W. Huynh, M. P. Conley, *Dalton Trans.* **2020**, *49*, 16453–16463; d) M.-C. Kervarec, T. Braun, M. Ahrens, E. Kemnitz, *Beilstein J. Org. Chem.* **2020**, *16*, 2623–2635; e) D. Cory, A. Wong, W. M. Ritchey, *J. Organomet. Chem.* **1982**, *235*, 277–285; f) X. Pan, M. Talavera, G. Scholz, T. Braun, *ChemCatChem* **2022**, *14*, e202200029.
[27] P. Juhás, T. Davis, C. L. Farrow, S. J. Billinge, *J. Appl. Crystallogr.* **2013**, *46*, 560–566.
[28] H. Riesemeier, K. Ecker, W. Görner, B. R. Müller, M. Radtke, M. Krumrey, *X-Ray Spectrom.* **2005**, *34*, 160–163.
[29] B. Ravel, M. Newville, *J. Synchrotron Radiat.* **2005**, *12*, 537–541.

Manuscript received: March 1, 2023
Revised manuscript received: March 3, 2023
Accepted manuscript online: March 8, 2023
Version of record online: March 24, 2023